The effect of wind and turbulence on sound propagation in the atmosphere

A. P. Oliveira

Instituto Superior Técnico, Technical University of Lisbon, Av. Rovisco Pais, 1049-001 Lisbon, Portugal

Abstract

In the last years, societies growing environmental and health conscience, obliged the national authorities to reinforce existing legislation concerning the maximum permissible noise levels. These new demands lead to increasingly accurate tools to perform noise analysis, not only because they must include a growing number of parameters that influence its propagation, thus with more complexity, but also with more flexibility, quick and easy use and less computational effort.

This dissertation, after presenting the several existing numerical methods to evaluate the sound propagation and its intrinsic limitations, describes the acoustic wave equation resolution method, using a Green function. Since the focus of this work is to develop a numerical application, which allows incorporating the wind and turbulence effects on sound propagation in the atmosphere, was created a C language numerical program. It includes input and output interfaces which ease the analysis of the referred effects variations on sound propagation.

The numerical program validation was achieved not only by comparing its results with exact numerical methods, but also by using numerical approaches with known accuracy and with results from experimental measurements. The program was applied to an airport by using realistic parameters. The coherent results obtained confirmed that the program developed is numerically accurate and its user interface is suitable and can be, easily and effectively, used to evaluate the effects of wind and turbulence on sound in the vicinity of an airport.

Keywords: Sound Propagation, Wind, Turbulence, Noise, Sound Refraction, Shadow Zone.

1 Introduction

The sound propagation studies in the atmosphere had always been a major concern in the scientific community. In the 19th century there were several isolated investigations to address specific requests, such as foghorns to aid shipping traffic or the location of artillery pieces. Refer to [Wescott & Kushner, (1965)], for a detailed bibliografy of the research done before 1965. When, in the 1960s, jet aircraft use grew significantly, governments throughout the world begun to produce specific legislation to limit the noise pollution, with the intent of protecting human health and minimizing the annoyance of noise to the communities and environment. As a result of this, new research activity grew in this area and with the aid of knowledge from other fields of physics, new methods to measure the outdoor sound propagation, with increasing accuracy, where developed.

The existent methods to calculate the sound level in a given atmosphere, have different degrees of complexity accuracy and speed. Some of them do not incorporate many parameters that influence the real atmospheric sound behavior or are computationally inefficient. The most relevant methods are the Generalized Fast Field Program (FFP) [Raspet, et al., (1985)], that do not incorporate range dependent atmospheric parameters; the Crank-Nicholson Parabolic Equation (CNPE) method [West, et al., (1992)], which requires significant computation time; the Ray Model [Gabillet, et al., (1993)], which results are not accurate enough for some situations and the Green Function Parabolic Equation (GFPE) method [Gilbert, et al., (1993)].

The GFPE method, which was developed by [Gilbert, et al., (1993)], is the most suitable one to study the effect of wind and turbulence on sound propagation in the atmosphere. Using this method, where we included several inputs that represent the most significant parameters of sound propagation phenomena, we developed a computational program, in C language, to calculate the sound field. This program puts together the best features of each of the three methods referred above.

2 Theoretical formulation

2.1 The GFPE method

As in previous studies, we consider a system with a monopole source, in a moving atmosphere with a non constant sound speed profile, above a finite impedance ground surface. Since most sound propagation programs, in particular the one developed in this text, use a two-dimensional representation of the atmosphere, an aproximation of the three-dimensional Helmholtz equation is required [Gilbert, et al., (1993)]. It is assumed that the system has azimuthal symmetry about the vertical axis z. Furthermore, a variable $q = p\sqrt{r}$ is defined, which removes the cylindrical spreading. Starting from the three dimensional Helmholtz equation, the resulting two dimensional far-field ($kr \gg 1$) equation is,

$$\frac{\partial^2 q}{\partial r^2}+\frac{\partial^2 q}{\partial z^2}+k^2(z)q=0 \tag{2.1}$$

where $k(z)=\omega/c(z)$ is the wave number, ω the angular frequency and c the speed of sound.

The derivation of the GFPE method uses the two dimensional version of the Kirchhoff-Helmholtz integral equation and the result is the Rayleigh II integral [Pierce, (1991)] for the field $q(\mathbf{R})$ at point $\mathbf{R_A}$, in terms of an integral over the vertical line at $r=r_0$. In the previous conditions, the Rayleigh II integral is,

$$q(\mathbf{R_A})=\frac{1}{2\pi}\int_0^\infty \left(q(\mathbf{R})\frac{\partial g(\mathbf{R};\mathbf{R_A})}{\partial r}\right)_{r=r_0} dz \tag{2.2}$$

where $\mathbf{R_A}=(r_A,z_A)$, $\mathbf{R}=(r,z)$ and the ground surface is located at $z=0$.

The Green's function $g(\mathbf{R},\mathbf{R_A})$ also satisfies the two-dimensional Helmholtz equation and can be written as follows,

$$\left(\frac{\partial^2}{\partial r^2}+\frac{\partial^2}{\partial z^2}+k^2\right)g(\mathbf{R},\mathbf{R_A})=-4\pi\delta(\mathbf{R}-\mathbf{R_A}) \tag{2.3}$$

where is assumed that the medium is independent of the horizontal distance r ($k=k(z)$) and g can be written as $g(\Delta r,z,z_A)$, with $\Delta r=r_A-r$ as the horizontal spacing. To express the Green's function in terms of the horizontal wave number k_h, the following Fourier transform is introduced,

$$G(k_h,z,z_A)=\int g(\Delta r,z,z_A)e^{-ik_h\Delta r}\,d\Delta r \tag{2.4}$$

The inverse Fourier transform formula,

$$g(\Delta r,z,z_A)=\frac{1}{2\pi}\int G(k_h,z,z_A)e^{ik_h\Delta r}\,dk_h \tag{2.5}$$

is now substituted in equation (2.2), with $r_A=\Delta r+r$ and $\partial_r=-\partial_{\Delta r}$. Taking into account Fourier transform properties, equation (2.2) results (changing the notation from z to z_A and from z' to z),

$$\begin{aligned} q(\Delta r+r,z)=&\frac{1}{4i\pi^2}\int_{-\infty}^{\infty}k_h e^{ik_h\Delta r}dk_h\\ &\int_0^\infty G(k_h,z',z)\,q(r,z')dz' \end{aligned} \tag{2.6}$$

The previous expression can also be derived from the spectral theorem of functional analysis [Gilbert, et al., (1993)]. The Green's function $G(k_r,z',z)$ also satisfies the transformed version of the Helmholtz equation [equation (2.3)],

$$\left(\frac{\partial^2}{\partial z^2}-{k_h}^2+k^2\right)G(k_h,z',z)=-4\pi\delta(z-z') \tag{2.7}$$

From equation (2.6), [Gilbert, et al., (1993)] derived the following expression for a refracting atmosphere,

$$\psi(r+\Delta r,z)=e^{i\Delta r\frac{\delta k^2(z)}{2k_a}} \tag{2.8}$$

$$\begin{aligned} &\frac{1}{2\pi}\left\{\int_{-\infty}^{\infty}\left[\Psi(r,k_z)\right.\right.\\ &+R_p(k_z)\Psi(r,-k_z)]\,e^{i\Delta r\left(\sqrt{k_a^2-k_z^2}-k_a\right)}e^{izk_z}dk_z\\ &\left.\left.+2i\beta\Psi(r,\beta)e^{i\Delta r\left(\sqrt{k_a^2-\beta^2}-k_a\right)}e^{-i\beta z}\right\}\right. \end{aligned}$$

where the spatial Fourier transform of $\psi(r,z)$ is,

$$\Psi(r,k_z)=\int_0^\infty \psi(r,z')e^{-iz'k_z}\,dz' \tag{2.9}$$

These two equations are the basic equations of the GFPE method. In equation (2.8), $R_p(k_v)=\left(k_vZ_g-k_0\right)/\left(k_vZ_g+k_0\right)$ is the plane wave reflection coefficient, Z_g is the normalized ground impedance, k_0 is the wave number at zero height, Δr is the horizontal spacing and $\beta=k_0/Z_g$.

In equation (2.8), the atmospheric refraction is considered by multiplying the solution in a non-refracting atmosphere by the exponential phase factor $\exp[i\Delta r(\delta k^2(z)/2k_a)]$, where the contribution factor $\delta k^2(z)$ is defined by,

$$k^2(z)=k_a^2+\delta k^2(z) \tag{2.10}$$

and k_a is a constant wave number at some average height. The second term on the right-hand side of equation (2.10) is the variation of the vertical profile, which can be either positive or negative and it is always small compared with $k^2(z)$.

Equation (2.8) represents the sum of three different types of sound waves. The first term represents the direct wave, the second term represents the wave reflected by the ground and the third term represents the surface wave.

2.2 Atmospheric turbulence

Atmospheric turbulence on sound propagation models is usually described using an effective sound speed that randomly fluctuates around an average value. Thus, we write the total refraction index as a deterministic part $n_d(z)$ plus a stochastic part $\mu(r,z)$,

$$n(r,z)=n_d(z)+\mu(r,z) \tag{2.11}$$

where $\mu\ll 1$, if weak turbulence is considered. Equation (2.11) considers that, although the fluctuating part μ to be, in reality, a function of both space and time, its value can be approximated in a specific instant of time. This approximation is called the frozen medium approach and it is possible because the sound waves travel so fast that the medium can be considered as 'frozen'.

Turbulence is included by multiplying equation (2.8) by an exponential factor, which includes the refractive index fluctuations $\mu(r,z)$ [Salomons, (2001)]. The exponential factor is [Martin, (1993)],

$$\exp(i\Theta) \tag{2.12}$$

where Θ is the turbulent phase fluctuation integrated over a range step, being its expression,

$$\Theta = k_a \int_r^{r+\Delta r} \mu(r,z)\, dr \tag{2.13}$$

Using the turbulent exponential factor in equation (2.12), the GFPE accurately takes into account the turbulent fluctuations within a range step.

The refractive index fluctuations function at the grid points is [Salomons, (2001)],

$$\mu(r,z_j) = \sum_{n=1}^{S} G(k_{nr},k_{nz}) \cos(rk_{nr} + z_j k_{nz} + \alpha_n) \tag{2.14}$$

where,

$$G(k_{nr},k_{nz}) = \sqrt{4\pi\ \Delta k\ F(k_{nr},k_{nz})\ k_n} \tag{2.15}$$

being $k_{nr} = k_n \cos(\theta_n)$, $k_{nz} = k_n \cos(\theta_n)$ and $k_n = n\Delta k$ for $n = 1,2,3 \ldots, S$. The angles θ_n and α_n are random numbers between 0 and 2π. These numbers are calculated using a pseudorandom number generator. The function $F(k_{nr},k_{nz})$ is the two-dimensional spectral density and can be either the Gauss spectrum or the von Kármán spectrum [Salomons, (2001)]. Replacing equation (2.14) into (2.13) results,

$$\Theta = \Upsilon(r+\Delta r, z_j) - \Upsilon(r,z_j) \tag{2.16}$$

with

$$\Upsilon(r,z_j) = k_a \sum_{n=1}^{S} \frac{G(k_{nr},k_{nz})}{k_{nr}} \sin(rk_{nr} + z_j k_{nz} + \alpha_n) \tag{2.17}$$

3 Numerical implementation

The GFPE method is a step by step extrapolation of the sound field $\psi(r+\Delta r, z)$ given by equations (2.8) and (2.9). A two dimensional rectangular grid is used, where Δr is the horizontal spacing and Δz is the vertical spacing. We use $\Delta z = \lambda/10$, where λ is the wavelength. The grid is limited by the ground surface at $z = 0$ and is truncated at the top at height $z = z_{top}$, where the total height of the atmosphere is given by $z_{top} = M\Delta dz$, being M a positive integer. To prevent unwanted reflection from sound waves at the truncated top surface, an absorption layer is located between $z = z_{abs}$ and $z = z_{top}$. The thickness of the absorption layer varies between 50λ and 100λ. This attenuation is obtained by adding an imaginary part $iA\left(z - z_{abs}/z_{top} - z_{abs}\right)^2$ to the wave number within the absorption layer, with A a factor that varies with frequency.

In order to allow an accurate comparison with other methods, we use a Gaussian starting field given by [Tappert, (1977)],

$$\psi(z) = \sqrt{k_a}\exp\left\{-\frac{k_a^2}{2}(z-z_s)^2 + \frac{Z_g - 1}{Z_g + 1}\exp\left[\frac{-k_a^2}{2}(z+z_s)^2\right]\right\} \tag{3.1}$$

where z_s is the source height above the ground.

To compute the sound field it is necessary to calculate several Fourier integrals in each range step. Each of the integrals can be approximated by a sum called Discrete Fourier Transform (DFT). For the Fourier integral represented by equation (2.9), the discrete sum is [Champeney, (1985)],

$$\Psi(r,k_n) \approx \left[\sum_{j=0}^{N-1} \psi(r,z_j) e^{-ik_n z_j}\right] \Delta z \tag{3.2}$$

where the integration variables k_z and z' are discretized respectively as,

$$k_n = n\Delta k, \qquad j = 0,1,2 \ldots . N/2, -N/2+1, -N/2+2 \ldots . -1 \tag{3.3}$$

$$z_j = j\Delta z \qquad j = 0,1,2 \ldots \ldots N-1 \tag{3.4}$$

being $\Delta k = 2\pi/(N\Delta z)$, Δz the vertical spacing and $N = 2M$ the Fourier transform size. As a consequence of Fourier transform's periodic nature, the vector elements $\Psi(r,k_n)$ and $\Psi(r,-k_n)$ can be related between them by a permutation of vector positions. Therefore, it is possible to include both integrals into a single transformation of size $N = 2M$, which is the double of the vertical grid size. This assumption decreases the computational effort. The integral $\Psi(r,\beta)$ only requires a single summation of N terms. After the above integrals have been evaluated, the inverse Fourier integral of equation (2.8) can be calculated with an approximation analogous to equation (3.2). Hence, the calculation of one range step requires two Fourier transforms: one forward DFT and one inverse DFT.

An alternative method for computing the Fourier integrals is based on the midpoint rule for numerical integration [Press, et al., (1986)]. The Fourier integral represented by equation (2.9) results in the following approximation,

$$\Psi(r,k_n) \approx \left[\sum_{j=0}^{N-1} \psi\left(r, z_j + \frac{1}{2}\Delta z\right) e^{-ik_n z_j}\right] e^{-\frac{1}{2}i\Delta z k_n} \tag{3.5}$$

where the integration variable k_z and z' are discretized as equation (3.3) and (3.4) respectively. Equation (3.5) uses the z coordinates at the center of the integration intervals $\left[z_j, z_{j+1}\right]$ therefore, the ground surface $(z = 0)$ is represented more accurately in equation (3.5) than in equation (3.2), which in turn leads to a more accurate approximation. For the inverse Fourier integral, an approximation analogous to equation (3.5) is used.

After each extrapolation step, $\psi(r,z_j) = 0$ for heights z_j where $j \in [M, N-1]$, as a way to avoid coupling between the top and ground surface, which can generate computational errors. These heights can be interpreted as corresponding to negative heights, due to the Fourier transform's periodic nature.

As we confirm in section 4.3, the accuracy of the method can be enhanced by using the following refraction factor,

$$\exp[i\Delta r\ \delta k(z)] \tag{3.6}$$

as a result, all computational simulations use this refraction factor.

The discrete sampling of the inverse Fourier transform causes errors when its summand oscillates rapidly. We multiply the summand by window function to suppress its rapid oscillation [Salomons, (1998)],

$$\begin{cases} 1 & \text{for } |k| < 0.5k_a \\ \cos^2\left(\dfrac{\pi(|k| - 0.5k_a)}{k_a}\right) & \text{for } 0.5k_a \le |k| \le k_a \\ 0 & \text{for } |k| > k_a \end{cases} \tag{3.7}$$

In section 4.3 we confirm that the use of this function improves the results accuracy.

The described numerical implementation and the additional functions, were included in the C language computational program. Its analysis and validation is performed in chapter 4, as well as, the results obtained.

4 Analysis and results

4.1 Test cases

This section defines various test cases to analyze the accuracy and optimization of the developed numerical implementation of the GFPE method.

The sound levels are measured using either the relative sound pressure or the transmission loss. The relative sound pressure ΔL is defined as the sound pressure level relative to the free field.

$$\Delta L = 10log_{10}\left(\frac{|p_c|^2}{|p_{free}|^2}\right) \tag{4.1}$$

The transmission loss (TL) is the sound pressure relative to the acoustic pressure of the direct sound field at 1 m from the source.

Table 4.1- Acoustic and environment parameters for two test cases in a non-refracting atmosphere.

Test case	1	2
Atmosphere	non-refracting $c_0 = 343$ m/s	non-refracting $c_0 = 343$ m/s
Ground surface	reflecting	absorbing
10 Hz	$Z_g = \infty$ (at all frequencies)	$Z_g = 51.94 + 51.73i$
100 Hz		$Z_g = 16.73 + 16.06i$
1000 Hz		$Z_g = 6.336 + 4.229i$
Source/receiver height	2 m	2 m

As known, in a non-refracting atmosphere the adiabatic sound speed is constant in all medium's points. The ground impedance of test case 1 ($Z_g = \infty$) represents a water surface while the ground impedances enumerated for the test case 2 represent grassland. They are calculated with the four parameter model of [Attenborough, (1985)]. These test cases have an exact analytical solution, which is fundamental to test the accuracy of the program.

The next test cases represent a more complex atmosphere, including atmospheric refraction. Their parameters are taken from benchmark problems used to test outdoor sound propagation models [Attenborough, et al., (1993)].

Table 4.3 displays the sound speed profiles of the four test cases. Test case 3 represents an idealized situation of sound propagation under upwind conditions. Test case 4 is similar to the previous one, only with opposite gradient sign and represents a downwind condition. Test case 5 is a DUC profile (downward - upward - constant) and is composed by three functions: a positive gradient up to 100 m, then a negative gradient between 100 and 300 m, followed by a constant profile. The gradient values are similar to the previous ones. Test case 6 is a logarithmic profile, which is used as a realistic representation of the atmosphere above open ground areas. Table 4.2 displays the remaining simulation parameters. The normalized ground impedance values are similar for the four test cases and are representative of grassland. They were calculated with the four parameter model of [Attenborough, (1985)].

Table 4.2 - Acoustic and environment parameters for a refracting atmosphere

Starting field	Gaussian
Ground surface	absorbing
1000 Hz	$Z_g = 40.16 + 39.97i$
100 Hz	$Z_g = 12.97 + 12.38i$
10 Hz	$Z_g = 5.03 + 3.18i$
Source height	5 m
Receiver height	1 m

4.2 Validation for a non-refracting atmosphere

With the parameters described in Table 4.1, we present the program results in Figure 4.1 plots, either the standard Fourier transform [equation (3.2)], or the alternate Fourier transform based on the midpoint rule for numerical integration [equation (3.5)]. Furthermore, we introduce the results with the exact solution, which numerically integrates an exact Laplace transform for a point source in a homogeneous atmosphere above an absorbing ground [Di, et al., (1993)]. All the results in this section use the relative sound pressure to measure the sound levels [equation (4.1)].

Table 4.3 - Atmospheric refraction parameters of four test cases.

Test case	3	4	5		6
Sound speed profiles speed c (m/s)	upward	downward	DUC		downward
	$343 - z/10$	$343 + z/10$	$343 + z/10$	$0 \le z < 100$	$343 + \ln(z/0.1 + 1)$
			$363 - z/10$	$100 \le z < 300$	
			333	$z \ge 300$	

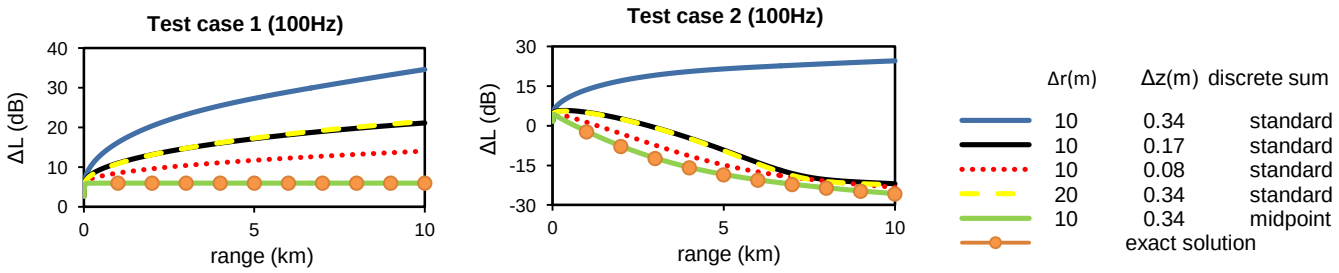

Figure 4.1 - Relative sound pressure up to 10 km with parameters from test case 1 (left figure) and test case 2 (right figure), for a 100 Hz point source.

The vertical spacing Δz should not be larger than $\lambda/10$ or 0.34 m in these two test cases. On the other hand, the horizontal spacing can be up to 50λ, depending on the simulation parameters. Acording to Figure 4.1, the sound level results, with the standard Fourier transform, deviate substantially from the exact solution. However, when using smaller vertical spacings, the latter results tend to approximate the exact solution. Oppositely, the error decreases with increasing horizontal spacing.

The alternate Fourier transform results, based on the midpoint rule, are very similar to the exact solution, presenting a difference minor than 0.1 dB. With $\Delta z = \lambda/10$, the standard transform deviates considerably. We found similar results for the frequencies 10 and 1000 Hz.

The alternate Fourier transform allows the use of larger Δz to obtain accurate sounds levels and consequently, the program requires a smaller number of vertical points. This results in a more efficient computational effort and, simultaneously, an accurate solution. For these reasons, all the following test cases use the alternate Fourier transform.

The discrete sampling of the inverse Fourier transform causes numerical errors due to the rapid oscillation of its summand. With the same conditions used in the previous test cases, we tested the window function's influence on sound levels and, simultaneously, compared them with the accurate results of the previous plots. We concluded that, with the window function, we can use larger range steps, up to 500 m, allowing a greater computational efficiency, without compromising the solution's accuracy.

4.3 Validation for a refracting atmosphere

Using the test cases from Table 4.3, we calculate the results and compare them with the CNPE method, as its accuracy is well known. From [Gilbert, et al., (1993)] we took, as reference, the range step values for the GFPE method, as well as, the reported range step values for the CNPE method.

Since the CNPE method sound levels are evaluated using the transmission loss (TL), we also used it to calculate the sound levels in the develop program. For all simulations we used a vertical spacing of $\Delta z = \lambda/10$. Test case 3 is represented by three frequencies as diplayed in Figure 4.3 plots,

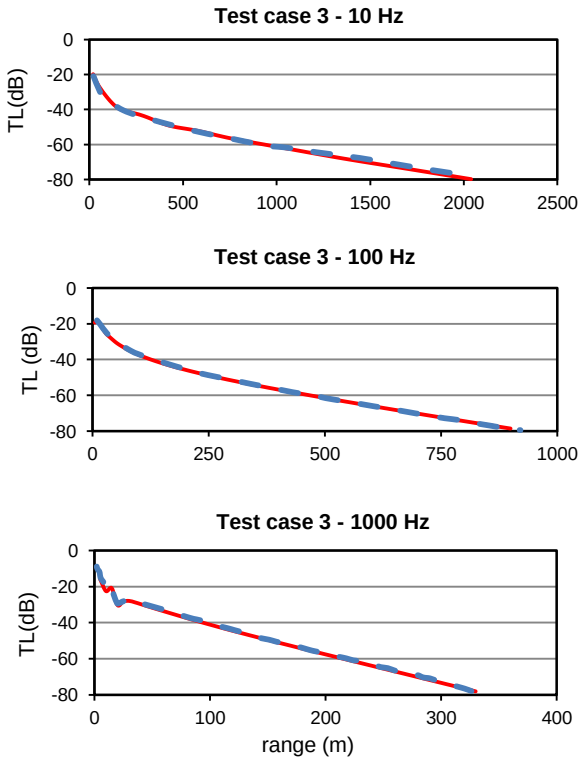

Test case 3	Range step (m)		
Frequency	10 Hz	100 Hz	1000 Hz
GFPE	200	100	30
CNPE	5	0.5	0.05

GFPE CNPE

Figure 4.2 - Comparison between the GFPE and the CNPE methods, with parameters from test case 3. The respective range steps used are displayed in the bottom table.

Despite a slight difference of 1 dB over a range of 1000 m for a frequency of 10 Hz, the compared results of the methods are in good accordance. By comparing the range steps on Figure 4.2, we conclude that the GFPE method range steps are 600, 200 and 40 times the ones of the CNPE method at 1000, 100, 10 Hz, respectively. This corresponds into a faster calculation, without sacrificing accuracy. We also verfied that larger range step values could be used successfully with small difference in the sound levels.

For test case 4, the two lines were mostly indistinguishable for all frequencies. The oscillatory

nature of the sound levels obtained, is a result of interference between the propagating modes.

In Figure 4.3, we study the accuracy of the GFPE method with a profile composed of three functions (test case 5). The agreement between the two methods is very good and both possess an oscillatory behavior for 100 and 1000 Hz. For the GFPE method, larger range steps can be used, with the disadvantage that the sound field oscillations can be inadequately represented. By comparing the range step values, we conclude that the GFPE method it is 40 to 163 times faster than the CNPE method.

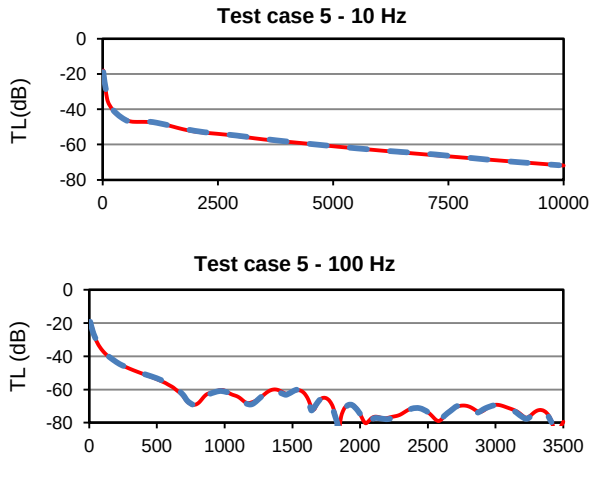

Test case 5	Range step(m)		
Frequency	10 Hz	100 Hz	1000 Hz
GFPE	200	35	10
CNPE	5	0.5	0.05

GFPE CNPE

Figure 4.3 - Comparison between the GFPE and the CNPE methods, with parameters from test case 5. The respective range steps used are displayed in the bottom table.

For test case 6, we studied the accuracy with a logarithmic sound speed profile and, simultaneously, we test the influence of the alternative refraction factor [equation (3.6)]. We compare both results with the CNPE method because it yields a solution of the wide angle parabolic equation, which is more accurate than the low angle parabolic equation used in the GFPE. The alternate refraction factor proved to be more accurate at long range than the standard refraction factor, which generates a phase error.

4.4 Turbulence analysis and results

In this section, we compare the numerical program developed with sound levels collected from a real atmosphere by [Weiner, et al., (1959)]. The data used to compare the program belongs to an extensive set of measurements of sound propagation, in an upward refracting atmosphere done by Weiner and Keast [Weiner, et al., (1959)].

The turbulence parameters for the two spectral density functions and for the refractive-index fluctuations (section 2.2), have to be correctly estimated to reproduce, as close as possible, the conditions of the experimental measurements. For the von Kármán and Gauss spectra we used a set of parameters for a turbulent atmosphere near a flat ground surface [Ostashev, (1997)]. To estimate the parameters of the refractive-index fluctuations is necessary to calculate the size of the sum S and the wave number spacing Δk in equation (2.17). Table 4.4 displays the parameters.

Table 4.4 - Turbulence parameters used

Gauss spectrum	von Kármán spectrum	Both spectra
$a = 1$	$\frac{C_T^2}{T_0^2} = 6 \times 10^{-7}\,\mathrm{m}^{-2/3}$	$S = 100$
$\frac{\sigma_T^2}{T_0^2} = 10^{-5}$	$\frac{C_v^2}{c_0^2} = 2 \times 10^{-6}\,\mathrm{m}^{-2/3}$	$\Delta k = 0.1\ \mathrm{m}^{-1}$
$\sigma_v^2 = 0$	$K_0 = 1\ \mathrm{m}$	$k_{\max} = 10\ \mathrm{m}^{-1}$

The measured values were corrected for spherical spreading and atmospheric absorption thus, we use the relative sound pressure to compare the results [equation (4.1)]. The sound levels were measured at a height of 1.5 m, up to a distance of 1400 m from the source, which was placed at a height of 3.7 m. Two frequencies were considered: 424 and 848 Hz. The sound speed profile is written as [Gilbert, et al., (1990)],

$$c(z) = \begin{cases} c_0 + b \ln\left(\frac{z}{d}\right), z \geq z_0 \\ c_0 + b \ln\left(\frac{z_0}{d}\right), z < z_0 \end{cases} \qquad (4.2)$$

where $c_0 = 340\ \mathrm{m/s}$, $z_0 = 0.01\ \mathrm{m}$ and $d = 6 \times 10^{-3}$. Two types of refraction where studied by [Weiner, et al., (1959)]: strong upward refraction and weak upward refraction. The first one refers to propagation almost directly upwind and the refraction parameter is $b = -2\ \mathrm{m/s}$. The second one represents the sound propagation mostly crosswind and $b = -0{,}5\ \mathrm{m/s}$.

The soil in the experimental measurement is described as a flat ground surface, covered with sparse vegetation. Using the empirical formulas of [Delany, et al., (1970)], the complex impedances for each source frequency are [Gilbert, et al., (1990)]: $8.00 + 9.24i$ and $5.17 + 5.57i$, for 424 and 848 Hz respectively.

Three different sound levels are presented in Figure 4.4. The connected red dots are the experimental sound levels. The solid lines are GFPE method solutions for a refracting turbulent atmosphere using either, the Gauss spectrum (green line, left side) or the von Kármán spectrum (blue line, right side). The dashed black lines are GFPE method outputs for a refracting atmosphere without turbulence

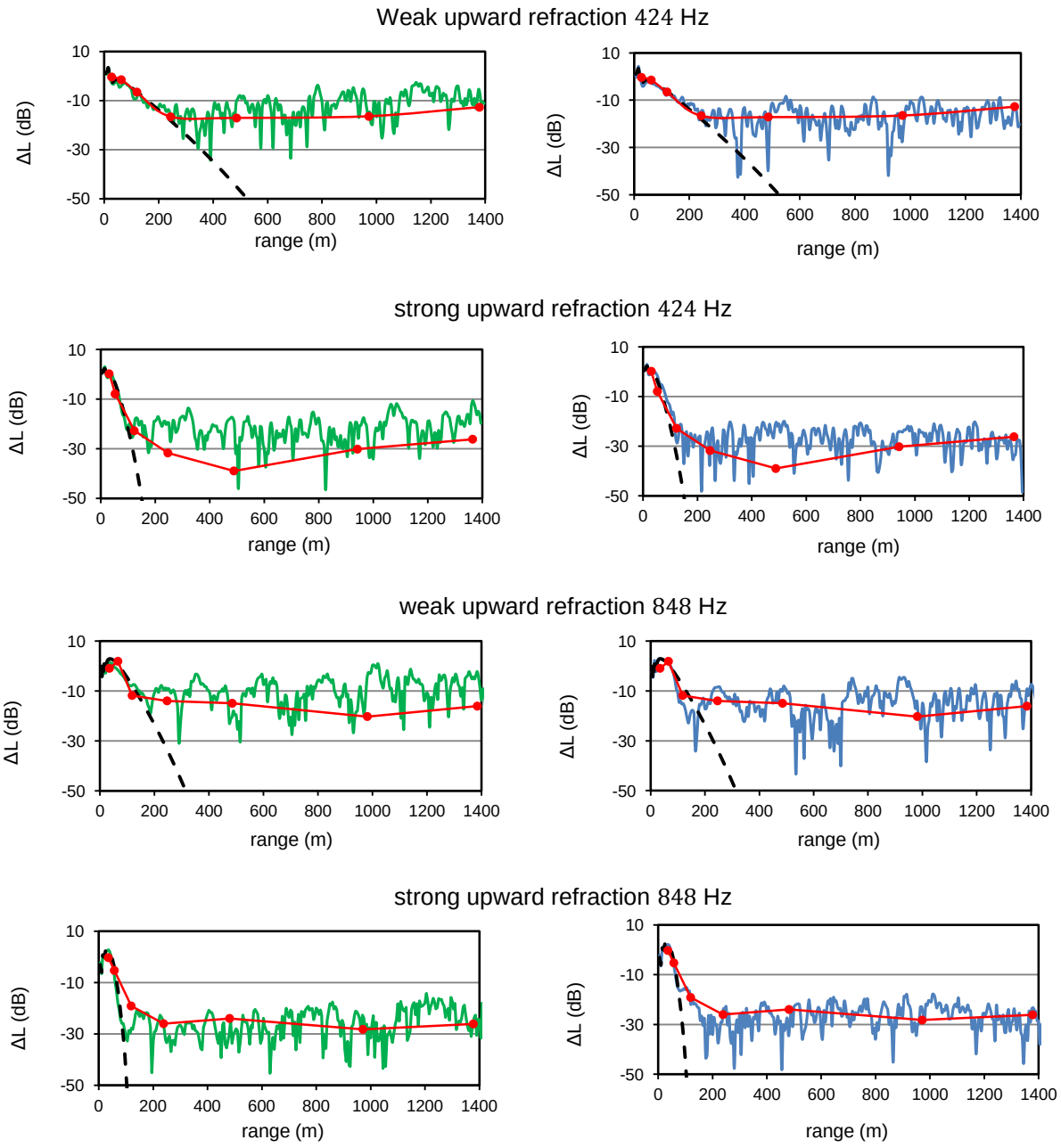

Figure 4.4 - relative sound pressure up to a range of 1400 m.

Overall, the results from the GFPE method with turbulence (green and blue solid lines) are in conformity with the experimental measurements (red connected dots), for both spectra. The exception is for strong upward refraction for 424 Hz, which differs 10 dB in the range from 500 m to 900 m. Additionally, for any of the test case, the average sound levels for several trials are consistent hence, one trial is enough to accurately estimate them.

Results from the GFPE method without turbulence (black dashed line) are severely underestimated for a distance greater than 200 m. Up to a range of 200 m, all the three results are in accordance. This means that turbulent effects are small up to this distance thus, at short range, sound propagation is mostly governed by deterministic parameters such as the source frequency or the refraction parameter. For long range sound propagation (more than 200 m), the incorporation of turbulence effects is essential in order to obtain realistic sound pressure levels.

5 Program application to an airport

In this section, we use the computational program developed to study the noise generated by an aircraft in the vicinity of an airport. This task requires information on air temperature and wind speed and direction, in the region where the sound propagates

5.1 Meteorological and simulation parameters

Several empirical formulas were developed by meteorologists to predict the wind and temperature gradients, when direct measurement is impractical or

unattainable. The formulas we use, are based on the Monin-Obukhov simularity theory [Monin, et al., (1979)]. Furthermore, we use Pasquill stability classes to classify different atmospheric conditions [Pasquill, (1961)].

We consider two meteorological conditions: light wind and moderate cloud cover (Pasquill class B) and moderate wind and moderate cloud cover (Pasquill class C). [Salomons, et al., (1994)] suggests evaluating Monin-Obukhov lenght L, using the Pasquill meteorological categories. Positive and negative values of L represent unstable and stable atmospheric conditions respectively. With a neutral atmosphere, L has infinite value. Moreover, turbulence has to be included in order to correctly estimate sound levels. We use the expressions sugested by [Zaporozhets, et al., (2011)] to estimate the Gauss spectrum parameters. The Monin-Obukhov profiles parameters and the Gauss spectrum parameters are displayed in Table 5.1 and Table 5.2, respectively.

Table 5.1 - Parameters used in the Monin-Obukhov profiles for two meteorological conditions

Pasquill Class	T_0 (K)	u^* (m/s)	T^* (K)	$1/L$ (m^{-1})	Stability
B	298	0.1	-0.33	-0.086	unstable
C	298	0.3	-0.11	-0.148	slightly unstable

Table 5.2 - Gauss spectrum parameters at a height $z = 1$ m

Pasquill class	a (m)	σ_T^2/T_0^2	σ_v^2/c_0^2
B	1	1.93×10^{-6}	2.86×10^{-7}
C	1	1.49×10^{-7}	2.58×10^{-6}

Two source heights were considered: 100 m and 2 m. The first one represents an aircraft taking off or landing, whereas 2 m stands for an aircraft taxiing. The wind direction proposed in Figure 5.1 was headwind or blowing against the direction of travel, since this is the most frequent and favorable situation when taking off or landing.

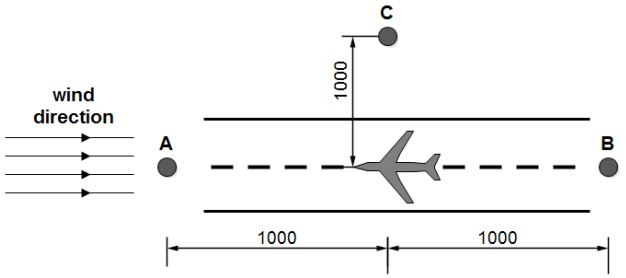

Figure 5.1 - Schematic representation of the source and receivers position (m) and wind direction.

We assumed three receiver locations, to simultaneously simulate upwind (receiver A), downwind (receiver B) and crosswind (receiver C) sound propagation. The receiver's height was set at 1.5 m to represent the typical human ear height.

The ground along the sound propagation path is a mixture of hardened asphalt, grassland and exposed soil. The normalized ground impedances Z_g for an octave band spectrum are displayed in Table 5.3 [Attenborough, (1985)]. Finally, Table 5.4 displays the test cases for the present study and their respective parameters.

5.2 Effect of atmospheric turbulence on sound propagation

One effect results in a spatial coherence loss that increases as the front waves propagate away from the source. This results into sound pressure fluctuations, from the average values. Plots from section 4.4 show this effect. The other effect occurs when an acoustical shadow region forms. Experimental measurements carried by [Weiner, et al., (1959)], show that sound levels in the shadow region are significantly higher than expected by the ray theory. It is generally assumed that atmospheric turbulence affects the maximum attenuation achieved in a shadow region [Piercy, et al., (1977)].

We use two different types of sound speed profiles, with upwind and downwind sound propagation, from Table 5.4, with class C atmospheric conditions. Figure 5.2 presents the results.

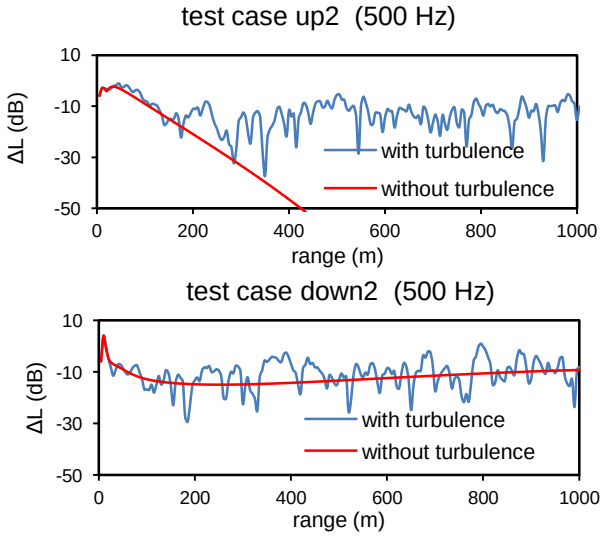

Figure 5.2 - One trial of the relative sound pressure up to a range of 1000 m, with and without atmospheric turbulence.

Table 5.3 - Normalized impedance values for an octave band spectrum

Frequency (Hz)	31.5	63	125	250	500	1000	2000
Normalized impedance	$29.4 + 29.0i$	$20.9 + 20.4i$	$15.0 + 14.3i$	$10.9 + 9.8i$	$8.1 + 6.6i$	$6.3 + 4.2i$	$5.3 + 2.5i$

Table 5.4 - Test cases and their respective parameters

Test case	up2	down2	cross2	up100	down100	cross100
Source height	2 m			100 m		
Receiver position	A	B	C	A	B	C
Receiver height	1.5 m					
Wind direction	upwind	downwind	crosswind	upwind	downwind	crosswind

With upwind propagation the sound speed decreases with height thus, a shadow region forms. The average sound levels relative to the free field remain constant throughout this region. When turbulence is not incorporated, the sound levels are largely underestimated.

With downwind propagation, the sound speed increases close to the ground therefore, the sound speed gradient is positive within this region. In this situation, the sound levels without turbulence are in accordance with the average ones with turbulence. In this particular case, the addition of atmospheric turbulence is redundant and not mandatory.

When the source is located at 100 m, the sound levels without turbulence and the average ones with turbulence are similar. Since the wind speed above a certain height is nearly constant, the sound speed gradient at a height of 100 m is only slightly negative. This explains why both the results are in close agreement, despite the fact that the sound waves are propagating in a negative sound speed gradient medium.

To graphically illustrate how turbulence influences the penetration of sound waves into the shadow region, we use the test case up2 from Table 5.4 and plot a two-dimensional representation of the relative sound pressure field, with (right plot) and without (left plot) turbulence effects.

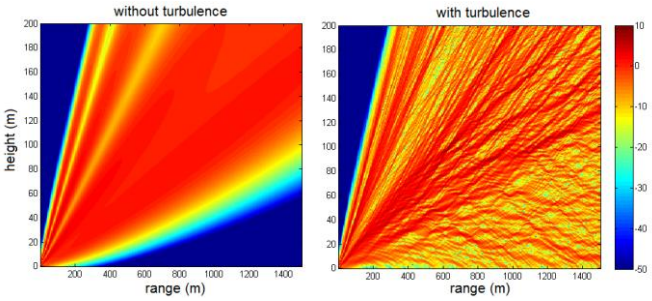

Figure 5.3 - Two-dimensional plots of the relative sound pressure level ΔL (dB). The frequency is 500 Hz

We obtained similar results for the remaining octave spectrum frequencies. These two-dimensional plots clearly show that sound pressure levels in a shadow region are a direct result of scattering due to atmospheric absorption. In their experimental study [Weiner, et al., (1959)] verified that the relative sound pressure levels, in the shadow region, were mostly independent of range. Furthermore, [Daigle, et al., (1986)] in the same conditions of the previous study, reported a limited dependence of relative sound pressure levels with height. These observations are in accordance with the results from the two dimensional plots in this section.

5.3 Effect of wind on sound propagation

To study the effect of wind on sound propagation, we use the test cases from Table 5.4, with B and C class atmospheric conditions. Moreover, turbulence is also included. The following two plots are for a source height of 2 m.

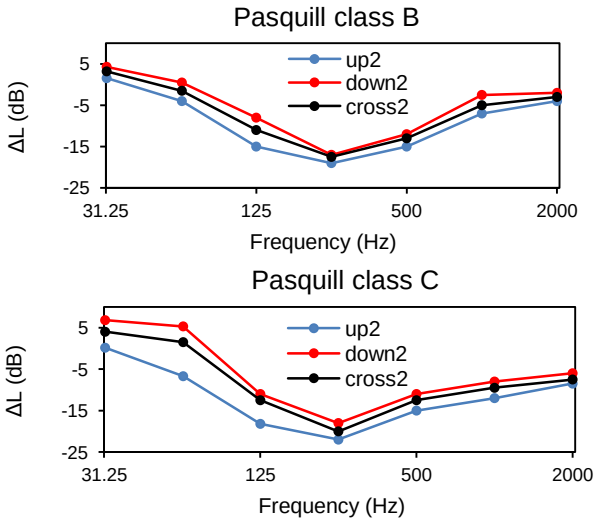

Figure 5.4 - Comparison of the relative sound pressure values, at a range of 1000 m, for three wind directions.

By comparing the wind directions in each plot, we infer that maximum attenuation is achieved when the wind is directly upwind. When the wind direction is downwind a sound speed inversion for moderate wind occurs, which by turn results in less attenuation of the sound waves. With crosswind propagation the attenuation value is between upwind and downwind propagation, as expected.

By comparing both meteorological conditions, we conclude that a stronger speed wind increases the attenuation on the sound levels and a light wind speed attenuates it less.

For a source height of 100 m, the attenuation achieved for a 1000 m range is smaller than the one for a source height of 2 m, for all test cases.

5.4 Airport scenario simulation: case studies

In the present section, we use the developed program to simulate two proposed scenarios, more realistic and complex. The first one simulates the noise emitted by an aircraft landing and the second one by an aircraft flying at a constant height.

Figure 5.5 illustrates case study 1, where an aircraft, initially at a height of 102 m, approaches the runway and lands (height of 2 m). The approach angle, also called glide slope, is approximately 3° above the horizontal.

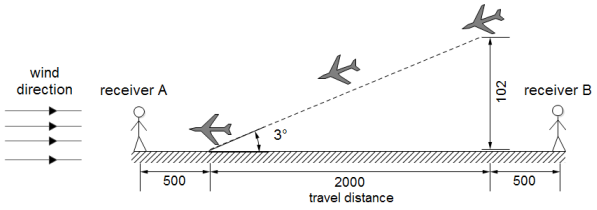

Figure 5.5 - Schematic representation of case study 1. All distances are displayed in meters.

We use different receivers to simulate different

wind directions (A upwind and B downwind). The receiver's height was set at 1.5 m to represent the typical human ear height.

Figure 5.6 illustrates case study 2, where we propose a scenario to simulate crosswind sound propagation. In this situation, an aircraft flies at a constant height of 20 m and the receiver C is positioned as displayed in Figure 5.6, at a height of 1.5 m.

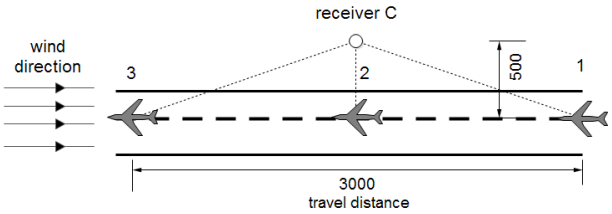

Figure 5.6 - Schematic representation of case study 2. The aircraft travels from position 1 to position 3 and all the distances are displayed in meters.

For the meteorological parameters we use both moderate wind and cloud cover from section 5.1. For the ground parameters, we use the normalized ground impedance values from Table 5.3.

Figure 5.7 displays the sound attenuation values due to geometrical spreading (black line), atmospheric absorption (red line) and meteorological and ground effects (blue line. The total attenuation (green line), is the sum of all combined effects.

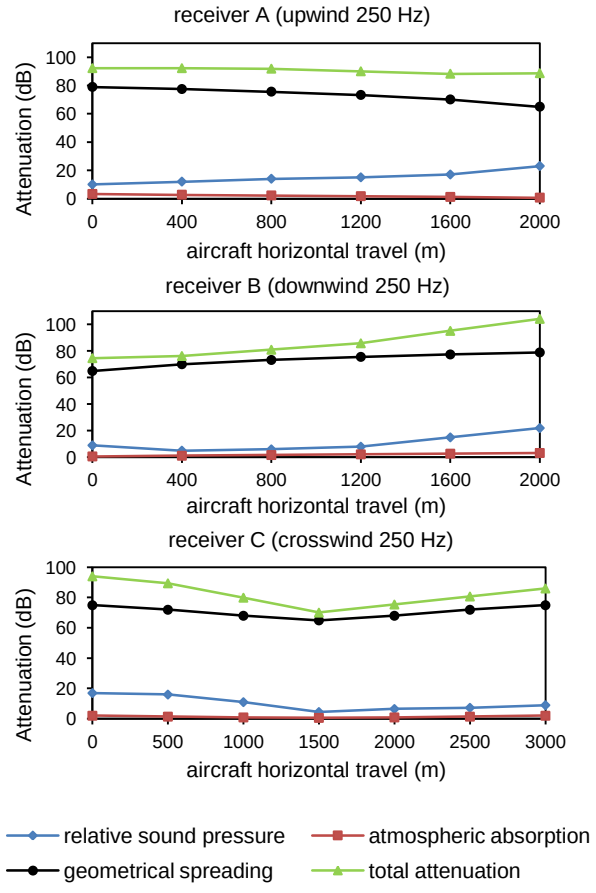

Figure 5.7 - Attenuation values for case study 1 (top two plots) and case study 2 (bottom plot).

For the receiver A, the distance between it and the aircraft decreases therefore, the atmospheric absorption and spherical spreading attenuation decrease with horizontal travel. Moreover, the relative sound pressure increases, since initially the source is at 102 m and its height decreases (up to 2 m), where the sound speed gradient is more intense.

For the receiver B the opposite occurs, the distance between the receiver and the aircraft increases hence, the atmospheric absorption and spherical spreading attenuation increase with horizontal travel. The relative sound pressure attenuation also increases, although with less intensity than for the receiver A (upwind propagation).

For the receiver C, the distance between the aircraft and the receiver decreases from 0 m up to 1500 m, where it reaches a minimum value, and then increases. The sound attenuation components also decrease up to 1500 m and afterwards increase. The relative sound pressure has more attenuation when the sound propagation is upwind (from 0 to 1500 m). When the propagation is downwind (from 1500 to 3000), the attenuation is less intense.

6 Conclusions and future developments

Since GFPE method does not allow an analytical solution, it was necessary to develop a numerical implementation (chapter 3) to solve the basic equations of the method (equations (2.8) and (2.9)). Several assumptions to develop the approach were introduced and justified. Some additional functions were also implemented, to overcome the limitations of the mathematical approach of the propagation physical phenomenon.

In chapter 4, three sets of test cases were used to validate the numerical implementation developed. The first set is for a non-refracting atmosphere, which has a mathematical exact solution; the second set includes atmospheric refraction and was compared with the CNPE method results; finally, the third set includes atmospheric turbulence in addition to the previous conditions and was verified by comparing with experimental measurements. In all the test situations, the results accordance between the numerical implementation and the mathematical and benchmark cases, were good enough to assure that the numerical approach and the program developed are accurate.

Finally, a real situation associated with an airport was simulated. Once again, it was confirmed that the program developed is numerically accurate and its user interface can be, easily and effectively, used to evaluate the effects of wind and turbulence on sound propagation in the vicinity of an airport.

To achieve a yet more realistic description, new features can be incorporated such as, ground barriers, topographic features and vegetation. A three dimensional approach, an inhomogeneous and anisotropic turbulence model, and a combined model of GFPE method with the Ray Model, to overcome the angular limitation of the first, are other possible improvements.

7 References

Attenborough, K. (1985). Acoustical impedance models for outdoor ground surfaces. *J. Sound & Vibration.* (1985), 99, pp. 521-544.

Attenborough, K., et al. (1993). Benchmark cases for outdoor sound propagation models. *J. Acoust. Soc. Am. (1993),* 97, pp. 173-191.

Champeney, D. C. (1985). *Fourier Transforms in Physics*. Bristol : Adam Hilger, (1985).

Daigle, G. A., Embleton, T. F. W. and Piercy, J. E. (1986). Propagation of sound in the presence of gradients and turbulence near the ground,. *J. Acoust. Soc. Am.* (1986), 79, pp. 613-627.

Di, X. and Gilbert, K. E. (1993). An exact Laplace transform formulation for a point source above a ground surface. *J. Acoust. Soc Am.* (1993), 93, pp. 714-720.

Gabillet, Y., et al. (1993). Application of the Gaussian Beam Approach to Sound Propagation in the Atmosphere: Theory and Experiments. *J. Acoust. Soc. Am.* (1993), 93(6), pp. 3105-3116.

Gilbert, K. E. and Di, X. (1993). A fast Green's function method for one-way sound propagation in the atmosphere. *J. Acoust. Soc. Am.* (1993), 94, pp. 2343-2352.

Gilbert, K. E., Raspet, R. and Di, X. (1990). Calculation of turbulence effects in an upward-refracting atmosphere. *J. Acoust. Soc. Am.* (1990), 87, pp. 2428-2437.

Martin, J. (1993). *Simulation of wave propagation in random media: theory and applications*. Washington : IOP Publishing and SPIE, (1993). pp. 463-486.

Monin, A. S. and Yaglom, A. M. (1979). *Statistical Fluid Mechanics: Mechanics of Turbulence.* Cambridge : MIT Press, (1979). Vol. 1.

Zaporozhets, O., Tokarev, V. and Attenborough, K. (2011). *Aircraft Noise Propagation: Assessment, Prediction and Control.* s.l. : CRC Press, (2011).

.

Ostashev, V. E. (1997). *Acoustics in Moving Inhomegeneous Media.* London : E&FN Spon, (1997).

Pasquill, F. (1961). The estimation of the dispersion of windborne material. *The Meteorological Magazine.* (1961), Vol. vol 90, pp. 33-49.

Pierce, A. D. (1991). *Acoustics: An Introduction to its Physical Principles and Applications.* New York : American Institute of Physics, (1991).

Piercy, J. E. and Embleton, T. F. W. 1977. Review of noise propagation in the atmosphere. *J. Acoust. Soc. Am.* 1977, 61(8), pp. 1403-18.

Press, W. H., Flannery, S. A. and Teukolsky, S. A. (1986). *Numerical Recepies: The Art of Scientific Computing*. Cambridge : Cambridge U.P., (1986).

Raspet, R. and Lee, S. W. (1985). A fast-field program for sound propagation in a layered atmosphere above an impedance ground. *J. Acoust. Soc. Am.* (1985), 77, pp. 345-352.

Salomons, E. M. (1998). Improved Green's function parabolic equation method for atmospheric sound propagation. *J. Acoust. Soc. Am.* (1998), 104, pp. 100-111.

Salomons, E. M., van den Berg, F. H. and Brackenhoff, H.E. A. (1994). Long-term average sound transfer through the atmosphere based on meteorological statistics and numerical computations of sound propagation. *Proceedings of the 6th International Symposium on Long Range Sound Propagation.* (1994).

Salomons, Erik M. (2001). *Computational Atmospheric Acoustics.* Netherlands : Kluwer Academic Publishers, (2001).

Tappert, F. D. (1977). *The parabolic approximation method*. [ed.] J. B. Keller and J. S. Papadakis. Springer-Verlag, Berlin : s.n., (1977). pp. 224-287.

Weiner, F. M. and Keast, D. N. (1959). Experimental study of the propagation of sound over ground. *J. Acoust. Soc. Am.* (1959), Vol. 31, pp. 724-733.

Wescott, J. W. and Kushner, S. S. (1965). *Propagation of Sound in the Air.* University of Michigan (AD 465 678) : A Bibliography with Abstracts, Report of Geophysics Lab, (1965).